Electronic Supplementary Material (ESI) for Physical Chemistry Chemical Physics.

SUPPORTING INFORMATION

Hydroxide promotes ion pairing in the $NaNO_2$-NaOH-H_2O system

Trent R. Graham,[†,*] Mateusz Dembowski,[†]
Hsiu-Wen Wang,[‡] Sebastian T. Mergelsberg,[†] Emily T. Nienhuis,[†]
Jacob G. Reynolds,[⸸] Calvin H. Delegard,[#] Yihui Wei,[§] Michelle Snyder,[†] Ian I. Leavy,[†]
Steven R. Baum,[†] Matthew S. Fountain,[†] Sue B. Clark,[†,§] Kevin M. Rosso,[†] Carolyn I. Pearce[†,δ,*]

† Pacific Northwest National Laboratory, Richland, Washington 99352, United States

‡ Oak Ridge National Laboratory, Oak Ridge, Tennessee 37831, United States

⸸ Washington River Protection Solutions, LLC, Richland, Washington 99352, USA

TradeWind Services, LLC, Richland, Washington 99352, USA

§ Department of Chemistry, Washington State University, Pullman, Washington 99164, United States

δ Department of Crop & Soil Sciences, Washington State University, Pullman, Washington 99164, United States

CORRESPONDING AUTHORS
*Trent R. Graham, E-mail: trenton.graham@pnnl.gov
*Carolyn I. Pearce, E-mail: carolyn.pearce@pnnl.gov

1.0 PREDICTION OF SODIUM NITRITE SOLUBILITY

In order to add an amount of sodium nitrite ($NaNO_2$) sufficient to exceed the solubility limit by a factor of about 1.3 for conditions described in **Table 1** of the manuscript, sodium nitrite solubility was estimated at 25°C in the absence of sodium hydroxide (NaOH), and sodium nitrite solubility was estimated at 25, 40, 60, and 80°C in 1, 3, and 6 moles·kg^{-1} NaOH solution. First, the solubility of $NaNO_2$ at 25°C was estimated by linearization of experimental data available in literature,[1] shown in **Figure S1** and **Equation S1**.

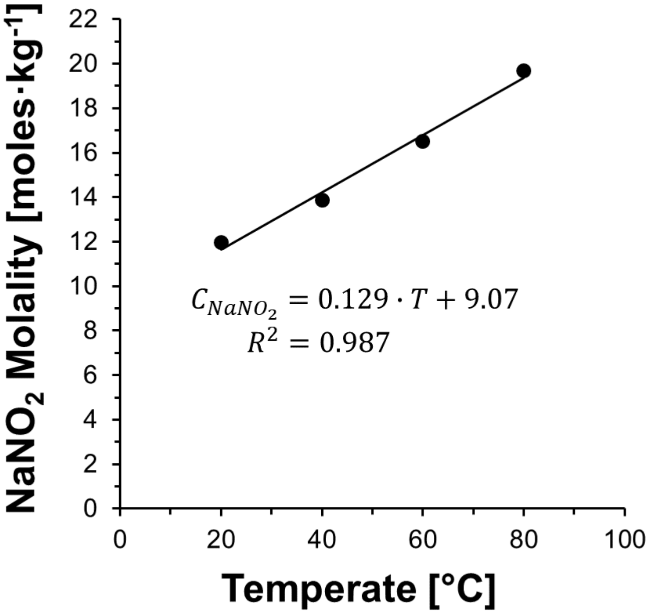

Figure S1. The solubility of $NaNO_2$ in H_2O in the absence of NaOH,[1] where the line is the regressed linear fit (**Equation S1**).

$$C_{NaNO_2} = 0.129 \cdot T + 9.07 \qquad \textbf{Equation S1.}$$

In **Equation S1**, C_{NaNO_2} is the concentration of $NaNO_2$ in units of moles·kg^{-1} and T is temperature in °C. The solubility of $NaNO_2$ in 1, 3, and 6 moles·kg^{-1} NaOH at 20 and 25°C was estimated by a linear and quadratic fit of literature data,[2] respectively. The selected data and regressed functions are shown in **Figure S2** and the regressed functions are shown in **Equation S2** and **S3**.

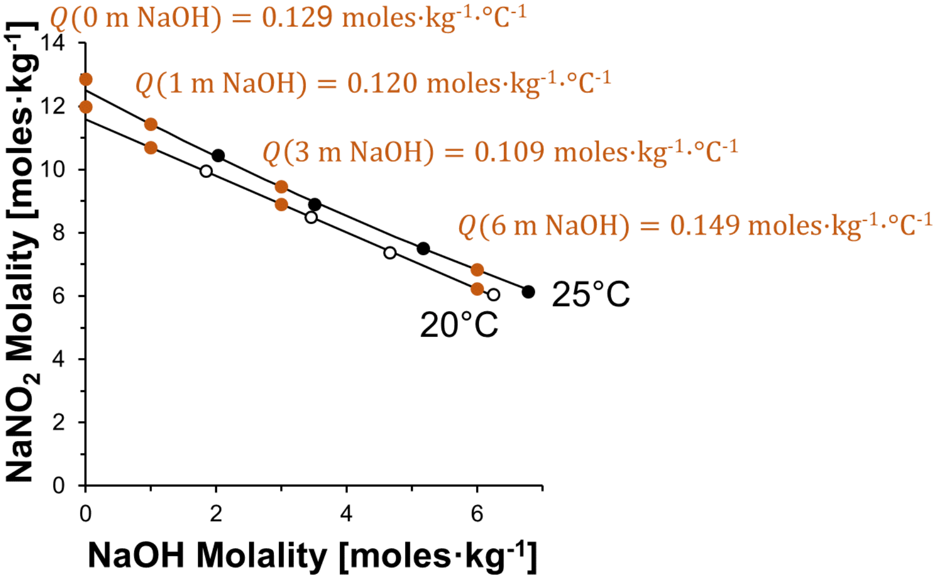

Figure S2. The solubility of $NaNO_2$ in NaOH solutions is shown for temperatures of 20 and 25°C.[2] The 20°C dataset is marked with unfilled symbols, the 25°C symbols are filled, and the orange symbols are the estimated $NaNO_2$ solubilities. The lines are the regressed linear and quadratic fit of the data (**Equations S2** and **S3**, respectively), and the fits have an R^2 of 0.9997 and 0.9986, respectively. The temperature dependence of $NaNO_2$ solubility (Q) is annotated for 0, 1, 3 and 6 moles·kg^{-1} $NaNO_2$ and is estimated with **Equation S4**.

$$C_{NaNO_2}(20°C) = -0.893 \cdot C_{NaOH} + 11.582 \qquad \textbf{Equation S2.}$$

$$C_{NaNO_2}(25°C) = 0.02387 \cdot {C_{NaOH}}^2 - 1.0893 \cdot C_{NaOH} + 12.500 \qquad \textbf{Equation S3.}$$

In **Equations S2** and **S3**, C_{NaOH} is the concentration of NaOH in units of moles·kg^{-1}. Based on the predicted solubility of $NaNO_2$ at 20 and 25°C in 0, 1, 3 and 6 moles·kg^{-1} $NaNO_2$, the temperature dependency of $NaNO_2$ solubility (Q) was approximated with **Equation S4**.

$$Q(C_{NaOH}) = \frac{d(C_{NaNO_2}(C_{NaOH}))}{dT} \approx \frac{C_{NaNO_2}(25°C, C_{NaOH}) - C_{NaNO_2}(20°C, C_{NaOH})}{25°C - 20°C}$$ **Equation S4.**

Given the fairly linear dependence of C_{NaNO_2} with temperature in solutions with no added NaOH (**Figure S1** and **Equation S1**), Q in NaOH-free solutions was estimated to be 0.129 moles·kg^{-1}·°C^{-1}. The other calculated Qs are annotated in **Figure S2**, where Q ranges between 0.109 and 0.149 moles·kg^{-1}·°C^{-1}, with an arithmetic mean ($\bar{Q}$) of 0.127 moles·kg^{-1}·°C^{-1}.

Using $\bar{Q}$, $NaNO_2$ concentrations at three NaOH concentrations (1, 3, and 6 moles·kg^{-1}) and at temperatures of 40, 60, and 80°C were predicted by linear extrapolation with **Equation S5**, and the predicted values are tabulated in **Table S1**.

$$C_{NaNO_2}(T, C_{NaOH}) = C_{NaNO_2}(25°C, C_{NaOH}) + \bar{Q} \cdot (T - 25°C)$$ **Equation S5.**

Table S1. Predicted Sodium Nitrite Solubilities in NaOH Solution

C_{NaOH} [moles·kg^{-1}]	Predicted C_{NaNO_2} [moles·kg^{-1}] 25°C	40°C	60°C	80°C
0	12.29	[a]	[a]	19.68[b]
1	11.43	13.33	15.87	18.40
3	9.45	11.35	13.88	16.41
6	6.82	8.72	11.26	13.79

(a) Given that experimental measurements of the solubility of $NaNO_2$ exists at 40 and 60°C,[1] no experiment was performed at these conditions, and the solubility was not predicted. Instead, control experiments determined the solubility of $NaNO_2$ with no added NaOH at temperatures of approximately 25 and 80°C, with results shown in **Table 1** and a comparison between predicted and experimental values also shown in **Figure S4**.

(b) Value corresponds to an experimental measurement in literature.[1]

The amount of $NaNO_2$ added to prepare the systems described in **Table 1** in the manuscript exceeded the predicted solubility in **Table S1** by a factor of about 1.3, which was enough in all cases to prepare systems with excess $NaNO_2$ solids. The prediction was found to correlate well with the measured data, with a correlation coefficient near unity, as shown in **Figure S3**.

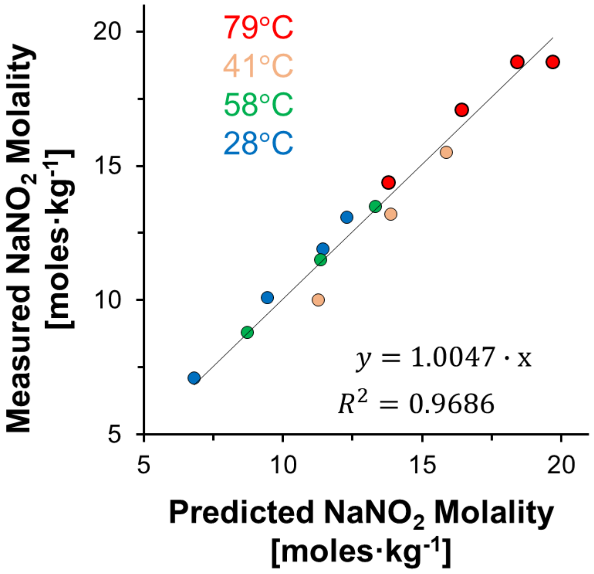

Figure S3. The correlation between the predicted and measured $NaNO_2$ solubilities is shown, where the line corresponds to a linear regression with a forced y-intercept of 0 using data acquired at all temperatures. The temperature in the legend corresponds to the experimental temperature, which is close but not identical to the temperature used in the prediction. The data are also recorded in **Table S1** and **Table 1**.

2.0 SOLUBILITY STUDIES

Approaching equilibrium conditions from different directions can be performed to validate the lack of kinetically slow processes. In this work, the solubility of sodium nitrite ($NaNO_2$) at 40°C was approached both by undersaturation, where solid $NaNO_2$ is dissolved until the solubility limit is reached, and from oversaturation. The approach from oversaturation is conducted by preparing a solution at 80°C and then by cooling this solution to precipitate $NaNO_2$ at a lower temperature. The results are shown in **Table S2**, where the good agreement between $NaNO_2$ molarities indicates that the systems were near equilibrium conditions when sampled.

Table S2. Comparison of the measured solubility of $NaNO_2$ approached from either undersaturation or oversaturation. A triplicate of solutions was prepared and the concentration of the nitrite ion was determined by ion chromatography. See the experimental methods section in the manuscript for additional details.

NaOH [g]	**$NaNO_2$ [g]**	**H_2O [g]**	**Temperature [°C]**	**Approach to solubility limit**	**Molarity $NaNO_2$ [moles·L^{-1}]**	**Density [g·cm^{-3}]**
4.0	116.6	100.0	41.1	Undersaturation	9.438(29)	1.375(1)
12.0	98.7	100.0	41.1	Undersaturation	8.199(44)	1.357(13)
24.0	78.0	100.0	41.1[a]	Undersaturation	6.459	1.340
4.0	161.5	100.0	80 to 40.5	Oversaturation	9.473(151)	1.359(3)
12.0	143.5	100.0	80 to 40.5	Oversaturation	8.251(0)	1.363(14)
24.0	125.6	100.0	80 to 40.5	Oversaturation	6.459(91)	1.365(1)

(a) Single measurement only.

Additional studies were undertaken to validate that filtering solutions did not influence the concentration of sodium nitrite measured in solution. This was done by preparing solutions of $NaNO_2$ in H_2O both under the solubility limit and concentrated slurries with solid $NaNO_2$ above the solubility limit. The concentration of nitrite in solution was then determined by (i) sampling the supernatant following sedimentation and (ii) by filtering the agitated suspensions. The results are shown in **Table S3** and **Figure S4**. Inspection of the data indicates that there is a near perfect correlation with a slope near unity between concentrations acquired with either method. Therefore, this result indicates that filtering $NaNO_2$ solutions likely does not influence the measured concentration.

Table S3. $NaNO_2$ was dissolved in H_2O and nitrite concentrations in molality (m, moles·kg^{-1}) were determined via a triplicate of ion chromatography measurements following either (i) filtering or by (ii) supernatant sampling following settling of the precipitate.

$NaNO_2$ (g)	**H_2O (g)**	**Temperature (°C)[a]**	**Molality $NaNO_2$ filtered (moles·kg^{-1})**	**Molality $NaNO_2$ supernatant (moles·kg^{-1})**
0.002	100.000	24.6	0.000299	0.000300
0.002	100.000	24.6	0.000315	0.000334
0.002	100.000	24.6	0.000301	0.000304
3.450	100.000	23.8	0.4820	0.4881

3.450	100.000	23.8	0.5058	0.5137
3.450	100.000	23.8	0.4868	0.4778
6.900	100.000	23.8	0.9927	0.9858
6.900	100.000	23.8	1.0273	1.0055
6.900	100.000	23.8	1.0110	1.0055
34.498	100.000	23.9	5.5616	5.5099
34.498	100.000	23.9	5.2725	5.3272
34.498	100.000	23.9	5.3610	5.4120
107.633	100.000	23.9	13.3145	12.8754
107.633	100.000	23.9	13.2379	13.1331
107.633	100.000	23.9	13.2287	13.4767

(a) Temperature stability of approximately 1 °C.

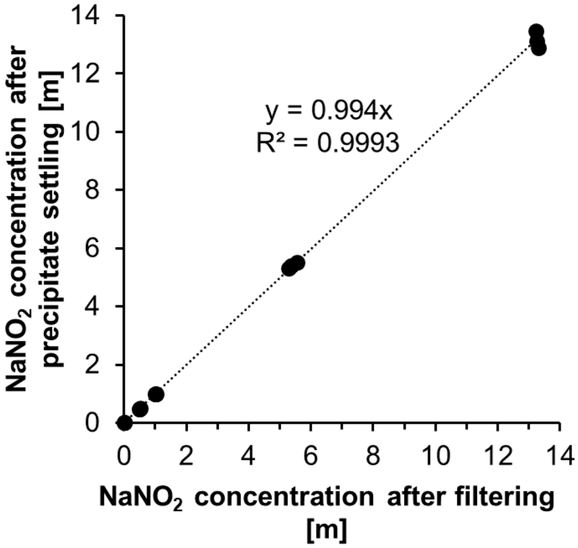

Figure S4. The solution concentration of nitrite by (i) filtering the system and by (ii) sampling supernatant after precipitate settling. The near unity between these molality (m, moles·kg^{-1}) measurements establishes the lack of filter matrix effects, as sodium nitrite concentrations of inhomogeneous systems containing excess crystalline $NaNO_2$ and homogeneous solutions fall on the same trendline.

3.0 SOLID STATE CHARACTERIZATION

The solid phase in equilibrium with solution in the $NaOH/NaNO_2/H_2O$ systems were studied for systems corresponding to entry row # 1, 4, 16, and 20 in **Table 1** in the manuscript. Systems were prepared at 20 and 80°C in an N_2-filled glovebox by the addition of 0 or 6 m (moles·kg^{-1}) NaOH solution to $NaNO_2$. After 2 days, the solids were collected with vacuum filtration and characterized with X-ray diffraction, Raman spectroscopy, and scanning electron microscopy. Analysis of the results, shown in Figures **S5** – **S7**, indicates that the phase in equilibrium with solution is anhydrous $NaNO_2$. This is consistent with prior literature that found that $NaNO_2$ hemihydrate is only stable below -5 °C.[3]

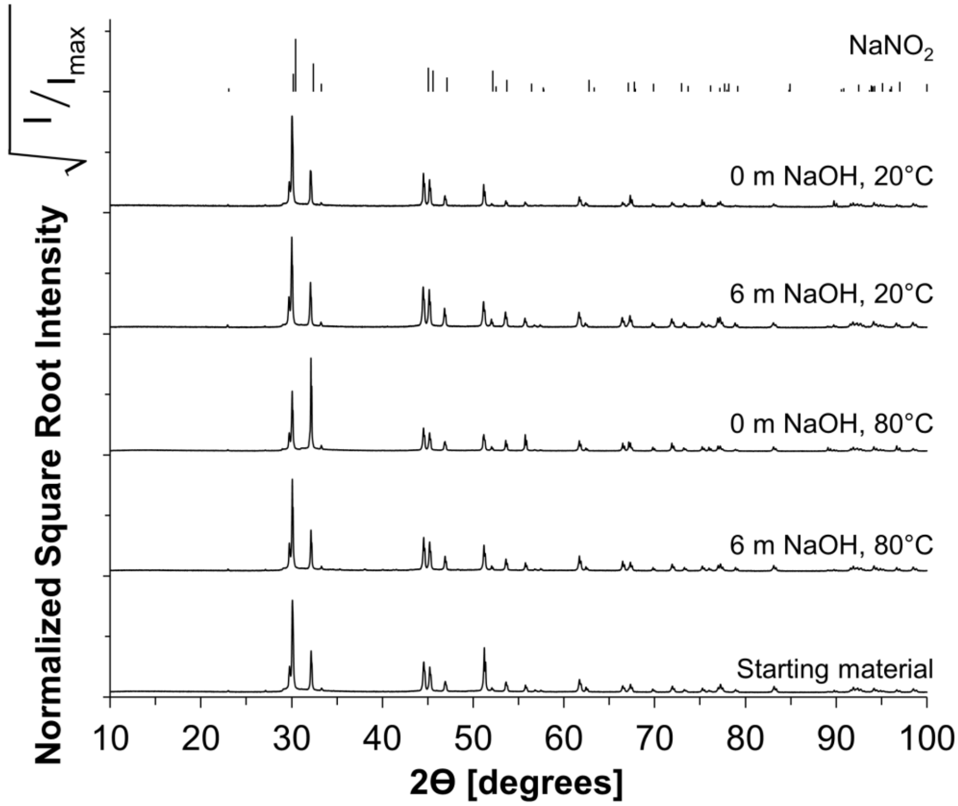

Figure S5. X-ray diffractograms were acquired on solids crystallized from saturated sodium nitrite solutions with 0 or 6 m (moles·kg^{-1}) NaOH, and at a temperature of 20 or 80°C. This approximately corresponds to entry row # 1, 4, 11, and 14 in **Table 1** of the main text. The results suggest that sodium nitrite is the crystalline phase obtained across system compositions and temperatures in this study, and the detected phase is consistent with prior literature studies that indicate that sodium nitrite hemihydrate is only stable at temperatures below -5°C.[3] The X-ray patterns are very similar to the starting $NaNO_2$ salt, which was dried at 80°C for two days before measurement. The diffractograms were acquired on a Rigaku Smartlab SE instrument, using a Cu sealed anode X-ray source (λ= 1.54056) operating at 40 kV and 44 mA, using a Θ-2Θ goniometer and a 1-dimensional semiconductor detector. The speed of acquisition was 1.8° min^{-1} with a step size of 0.01°. The diffractograms are offset and normalized to the square root intensity of the maximum reflection. The expected reflections of $NaNO_2$[4] are also shown in units of square root intensity.

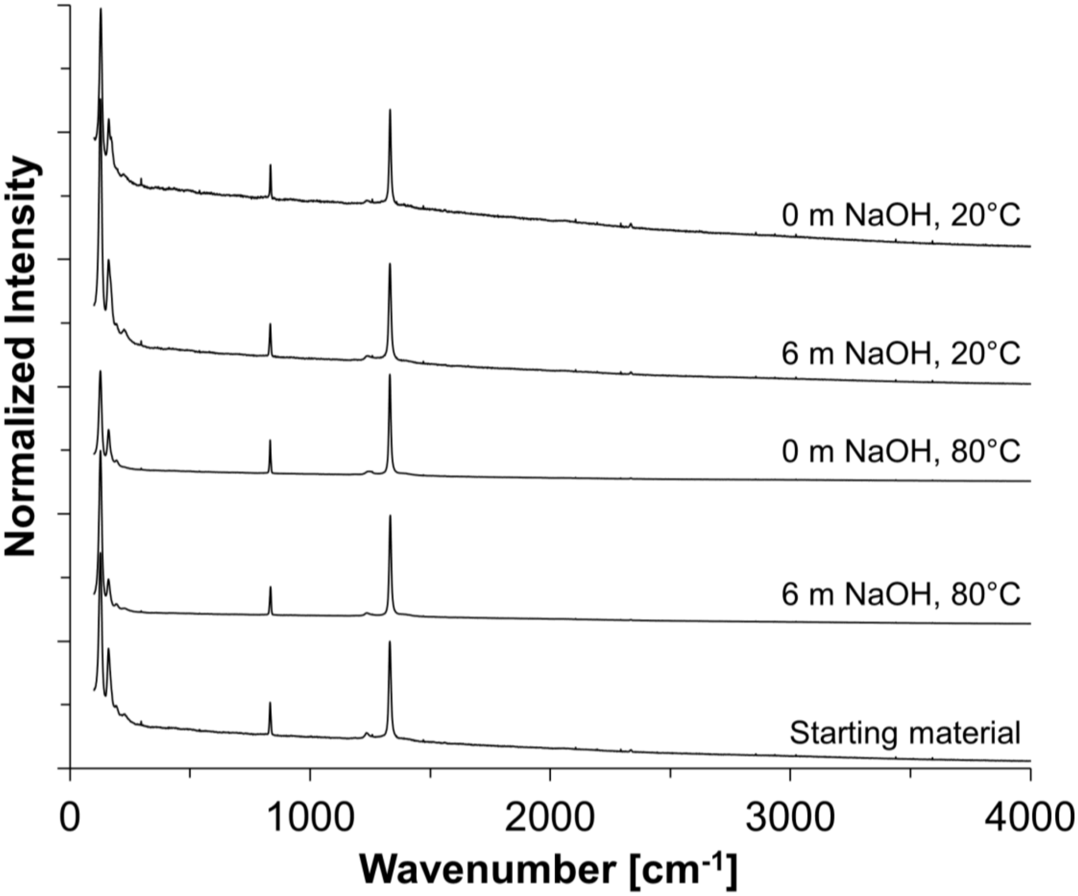

Figure S6. Raman spectra were acquired on solids crystallized from saturated sodium nitrite solutions with 0 or 6 m (moles·kg^{-1}) NaOH, and at a temperature of 20 or 80°C. This approximately corresponds to entry row # 1, 4, 11, and 14 in **Table 1** of the main text, respectively. The results suggest that sodium nitrite is the crystalline phase obtained across system compositions and temperatures in this study, and the detected phase is consistent with prior literature studies that indicate that sodium nitrite hemihydrate is only stable at temperatures below -5°C.[3] The consistent Raman spectra across system conditions is in agreement with the XRD on these solids, and the Raman spectra of the starting $NaNO_2$ salt material are very similar to spectra collected following vacuum filtration. The lack of water bending modes and the absence of OH-stretching modes indicates that sodium nitrite hemihydrate and sodium hydroxide hydrate are not present. The Raman spectra were acquired on a Horiba HR Raman spectrometer, using a 632.81 nm laser source and a 40× objective. The spectra were collected between 100 – 4000 cm^{-1} using the average of 10 acquisitions with an exposure time of 30 s. The spectra are normalized to the maximum peak height of the band near 1330 cm^{-1}.

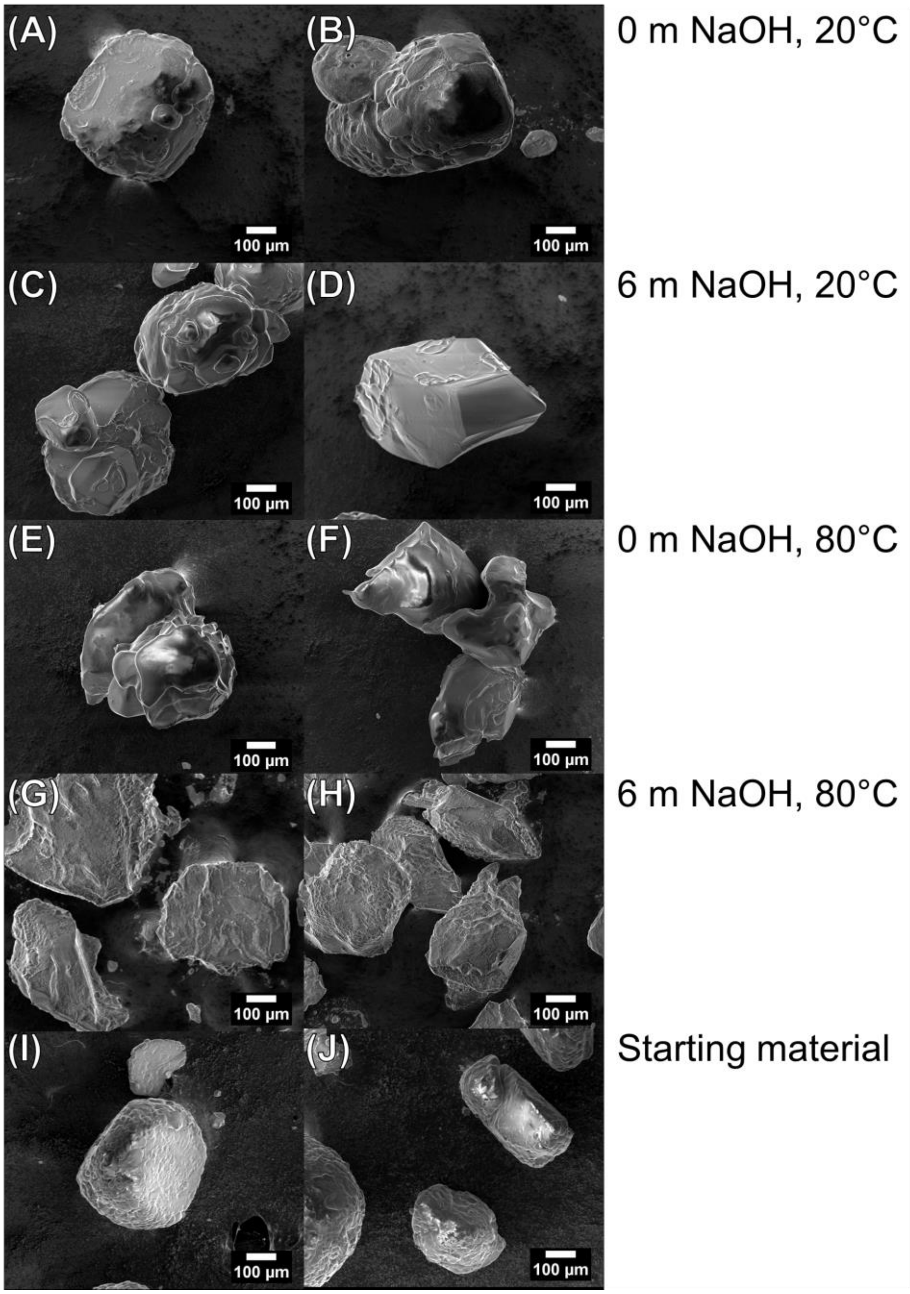

Figure S7. Scanning electron micrographs were acquired on solids crystallized from saturated sodium nitrite solutions with 0 or 6 m (moles·kg^{-1}) NaOH, and at a temperature of 20 or 80°C. The system conditions approximately correspond to entry row # 1, 4, 11, and 14 in **Table 1** of the main text. The respective micrographs are (A, B), (C, D), (E, F), and (G, H) with the starting $NaNO_2$ material shown in (I, J). The results indicate that sodium nitrite aggregated crystals are in excess of a hundred microns. The micrographs were acquired using a Helios NanoLab 600i SEM (FEI, Hillsoboro, OR), with a 3.0 kV acceleration voltage and a 0.17 nA current, and processed in ImageJ (v1.51, Released April 23, 2018), where the contrast was enhanced by 0.3 % and the scale bar graphic was inserted.

4.0 SOLUTION STATE RAMAN SPECTROSCOPY

To probe the chemical environment of the NO_2^-, OH^-, Na^+, and H_2O in saturated solutions, Raman spectroscopy was performed. The solutions, which are described in entries 1 – 4 in **Table 1** of the manuscript, are listed in **Figure S8**. For anhydrous $NaNO_2$ crystals, bands assigned to the symmetric stretch (ν_1), antisymmetric stretch (ν_3), and deformation (ν_2) of the NO_2^- ion occur at 1326, 1250, and 829 cm^{-1}, respectively.[5,6] This is consistent with the results shown in **Figure S6**. In aqueous solutions of $NaNO_2$, the bands of NO_2^- ions occur at 1331, 1242, and 817 cm^{-1}, and are similarly and respectively assigned to the symmetric stretch, antisymmetric stretch, and deformation of the NO_2^- ion.[7] Of these bands, the deformation band, v_2, is relatively sensitive to the presence of ion pairs.[6,8]

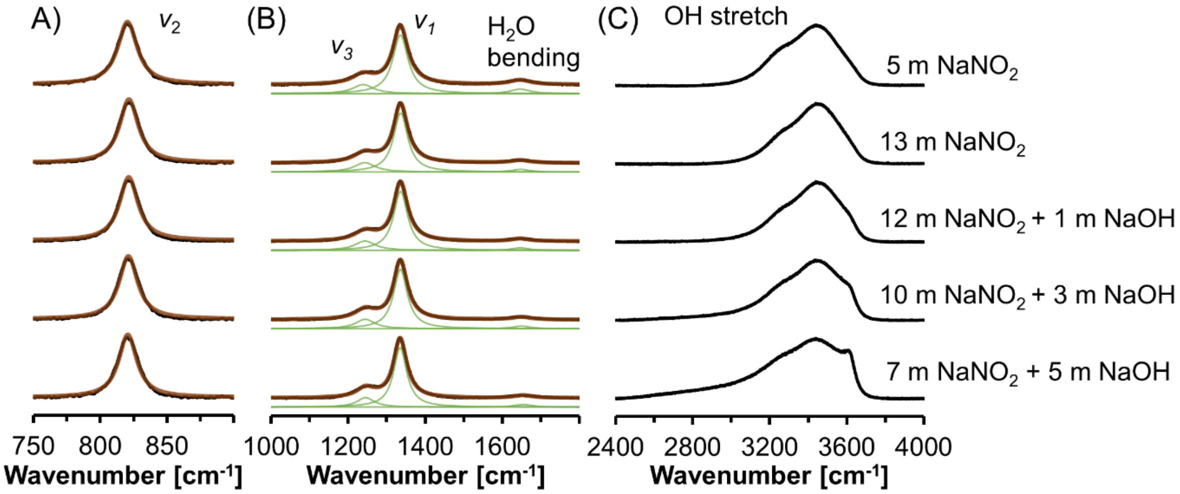

Figure S8. Raman spectra of the subset of solutions, where the brown line shows the sum regressed Lorentzian line shape fit, the green lines show the individual components, and the data are shown in black. The data in each spectral region are normalized to the same maximum peak intensity. Traces shown for (A) deformation band (B) symmetric and asymmetric stretch bands, and (C) hydroxide stretching region.

Figure S8A shows the Raman spectra of the $NaNO_2$ solutions, where the deformation band can be fit by a single Lorentzian function. The absence of additional resolved bands near 800 cm^-

[1] for all compositions indicates a lack of strong ion-pair interactions or that ion-pair species exhibit very similar deformation band wavelengths. In studies with divalent cations, distinct ion-paired species can be resolved via deconvolution of partially resolved deformation bands, and this has been leveraged to interrogate both cadmium nitrite interactions[6] and also calcium/magnesium nitrite interactions in water.[8] For example, a second deformation band occurs at 860, 840 and 830 cm^{-1} for ion-paired NO_2^- to cadmium, magnesium, and calcium ions, respectively, suggesting the wavenumber of the distinct deformation band of ion-paired NO_2^- is inversely correlated to the atomic number of the cation.[6,8] The occurrence of a second Raman band attributed to strong ion pairing also manifests in solutions of other nitrogen oxyanions. This is seen in, for example, zinc nitrate methanolic solutions, where a second well resolved Raman band appears at 753 cm^{-1} wavenumbers shifted from the v_4 with respect to D_{3h} symmetry vibration of the NO_3^- ion at 715 cm^{-1},[9] or in aqueous $NaNO_3$ solutions, where the NO_3^- asymmetry emerges for the v_4 vibration,[10] with correlated progressive shifts for peaks at 1000 cm^{-1}.[11]

Specific to solutions of alkali nitrites, a similar systematic perturbation of the appearance of the deformation band assigned to ion pairs composed of NO_2^- and Li^+, Na^+, K^+, Rb^+, and Cs^+ correlated with a decrease in wavenumber of the band assigned to ion pairs near 800 cm^{-1}. This trend is seen in both ammonia[12] and water.[7,13] However, for $NaNO_2$ aqueous solutions, there is little to no asymmetry of the v_2 band across a wide range of concentrations,[7,13] which is unlike the aforementioned Raman spectra of magnesium, calcium, and cadmium nitrite solutions.[6,8] The Raman spectra in **Figure 8A** are also consistent with those for mixtures of 1.25 M (moles·L^{-1}) $NaNO_2$ and 0.25 M $NaNO_3$, where addition of NaOH did not result in the emergence of any asymmetry in the deformation band.[14] Instead, the v_2 band fwhm was found to be weakly sensitive to Na^+ concentration, decreasing from 18 cm^{-1} with no added NaOH to 16 cm^{-1} upon addition of

14.5 M NaOH.[14] A similar decrease in fwhm on the order of a few wavenumbers for the v_2 bands is obtained in this work, with values shown in **Figure S9**.

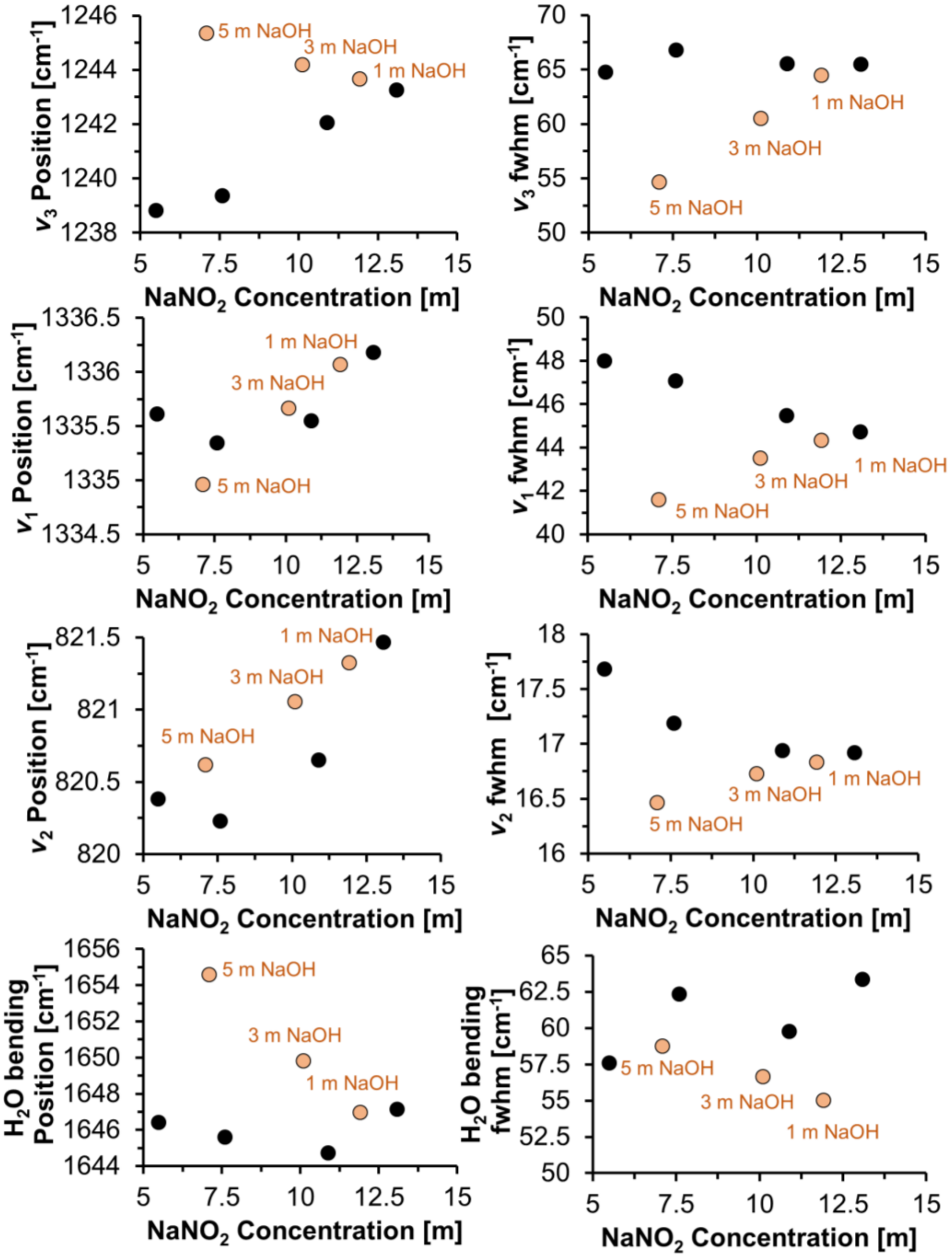

Figure S9. Lorentzian line shape parameters for sodium nitrite solutions (filled data points) and sodium nitrite with sodium hydroxide (orange data points). The datapoints of the solutions that include sodium hydroxide are annotated with the concentration of sodium hydroxide. The concentration of $NaNO_2$ and NaOH are in units of molality (m, moles·kg^{-1}).

5.0 TABULATED DIFFUSION COEFFICIENTS

Diffusion coefficients acquired with pulsed field gradient, diffusion-ordered nuclear magnetic resonance spectroscopy are listed in **Table S4**. The error associated with the diffusion coefficient originates from the residual obtained by fitting Stejskal-Tanner relationship[15,16] in vNMRJ to the integrated resonance as a function of pulsed field gradient strength.

Table S4. ^1H and ^{23}Na diffusion coefficients (D) acquired with pulsed field gradient NMR spectroscopy at a field strength of 17.6 T and a temperature of 25°C.

$NaNO_2$ [moles·kg^{-1}]	NaOH [moles·kg^{-1}]	^{23}Na D [10^{-10} m^{2}s^{-1}]	^{1}H D [10^{-10} m^{2}s^{-1}]
5	0	9.8(2)	14.3(3)
13	0	5.9(2)	7.8(4)
12	1	5.5(3)	7.3(2)
10	3	4.7(2)	5.8(1)
7	5	3.6(2)	4.1(1)

6.0 ADDITIONAL X-RAY PAIRWISE DISTRIBUTION FUNCTION ANALYSES

To compare the data presented in **Figure 6** in the manuscript to crystalline solids, X-ray PDF profiles were calculated from previously published crystallographic data of α-NaOH, β-NaOH, γ-NaOH, $NaOH \cdot H_2O$, and $NaNO_2$.[4,17,18] The crystal structures are shown in **Figure S10** and the G(R) data is shown in **Figure S11**. In general, the modeled fit captures most of the atom pair distances in the short-range order of the samples, however medium-range and long-range order are incongruent, as shown when comparing $G(R)\cdot R^2$ of the solutions with G(R) of the solid phases.

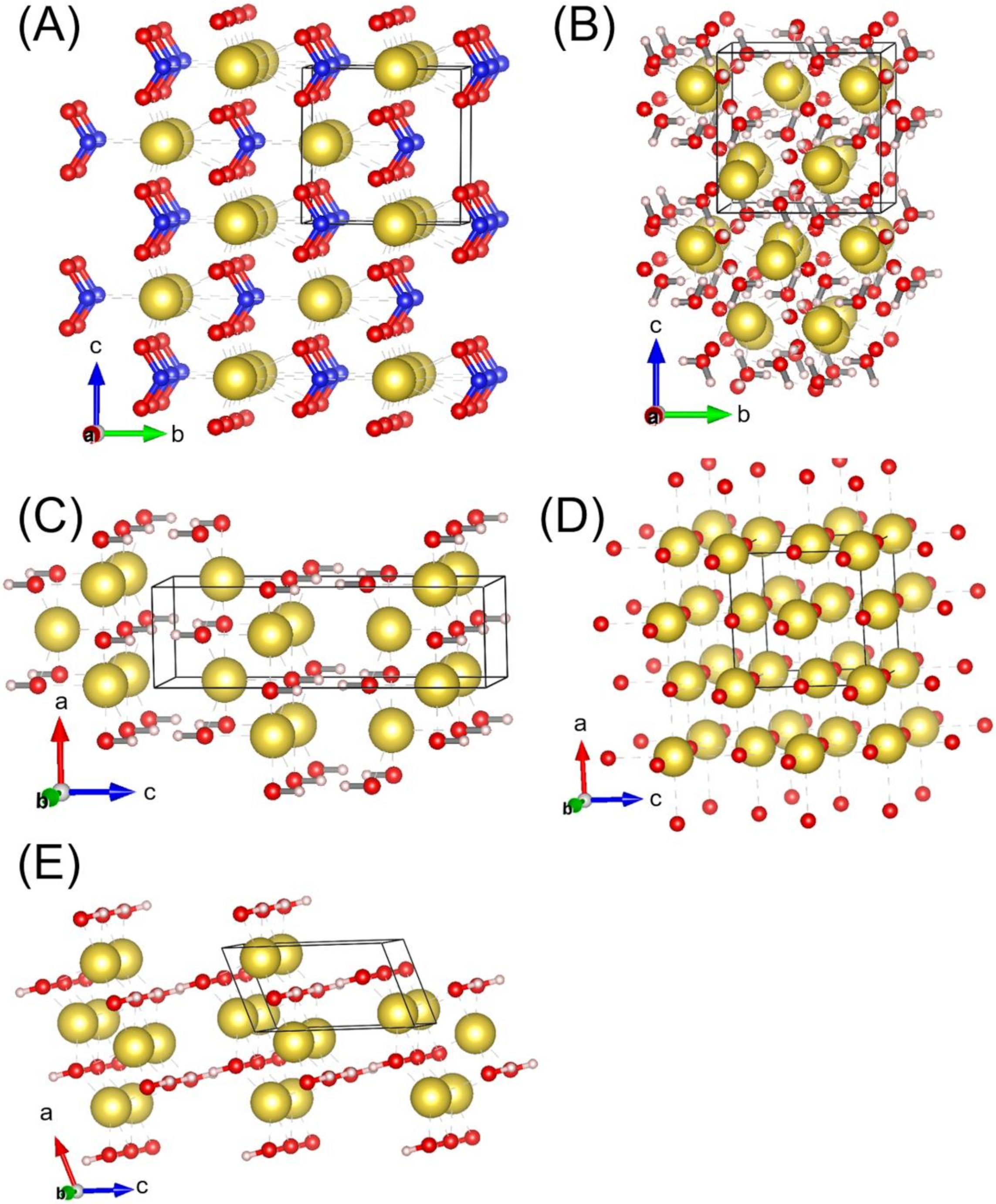

Figure S10. Crystal structures are drawn for visualization of phases selected for simulation of G(r) X-ray PDF data. The crystal structures are (A) $NaNO_2$ (B) $NaOH{\cdot}H_2O$, (C) α-NaOH, (D) β-NaOH, and (E) γ-NaOH.[4,17,18] Sodium atoms are drawn in yellow, oxygen in red, hydrogen in pink/white, and nitrogen in blue. The software used to draw the crystal structures is Visualization for Electronic and STructural Analysis (VESTA, v3.4.4, build date March 28, 2018).

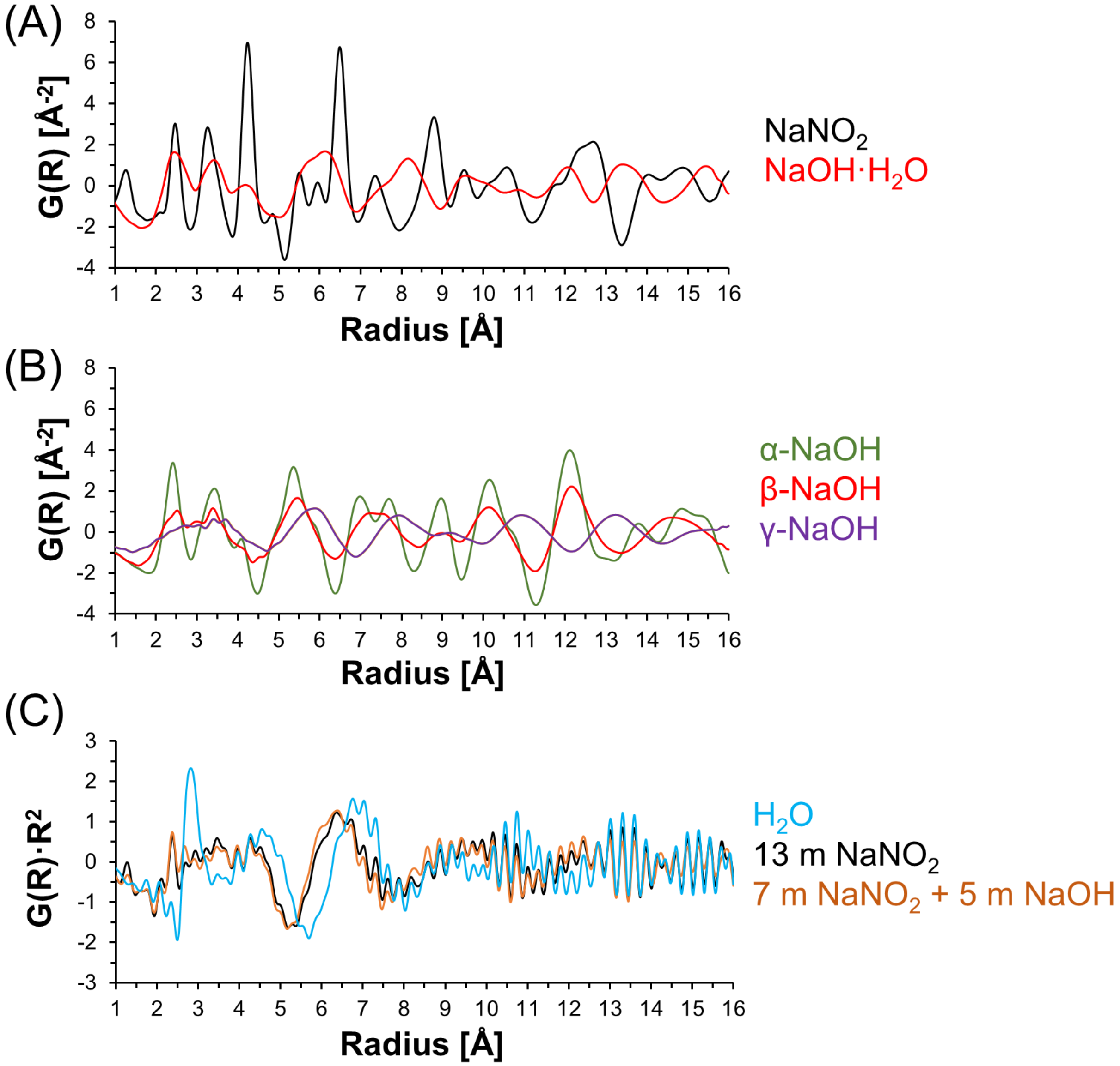

Figure S11. Simulated X-ray PDF results and comparison to experimental data. (A) Simulated X-ray PDF of crystalline $NaNO_2$ and $NaOH \cdot H_2O$. (B) Simulated X-ray PDF of α-, β- and γ-NaOH. (C) Scaled experimental G(R)·R^2 of Kapton-subtracted solution samples. PDF profiles of short-range ordered materials, such as solutions and glasses, are commonly scaled to highlight density-corrected medium- and long-range features beyond the apparent coherence limit. Simulated PDF profiles were calculated using DISCUS[19] with the following instrumental parameters: Q_{damp} = 0.040217, Q_{broad} = 0.015487. Instrumental parameters were refined for a CeO_2 standard using PDFgui[20] with R_{wp} = 12.59 % and reduced χ^2 = 0.003703. The Q_{max} value was fixed at 24.26 Å^{-1}, in accordance with the experimental data. All solids were modeled as 10 nm x 10 nm x 10 nm particles, in order to avoid size-dependent dampening.

REFERENCES

1 E. Washburn, International Critical Tables of Numerical Data, Physics, Chemistry and Technology, New York, New York, 1928.

2 V. F. Plekhotkin and L. P. Bobrovskaya, *Russ. J. Inorg. Chem.*, 1970, **15**, 842–844.

3 A. M. Babenko, The Urea-Sodium Nitrite-Water System, *Russ. J. Inorg. Chem.*, 1971, **16**, 1489–1491.

4 T. Gohda, M. Ichikawa, T. Gustafsson and I. Olovsson, X-ray study of deformation density and spontaneous polarization in ferroelectric $NaNO_2$, *Acta Crystallogr. Sect. B Struct. Sci.*, 2000, **56**, 11–16, DOI:10.1107/S010876819901054X.

5. H. H. Eysel, C. W. Von Der Lieth, G. Bertsch and M. H. Brooker, Intensities of polarized raman spectra of single crystal sodium nitrite and correlation with intensities of the aqueous ion, *Mol. Phys.*, 1981, **2**, DOI:10.1080/00268978100102521.

6 D. E. Irish and R. V. Thorpe, Raman Spectral Studies of Cadmium–Nitrite Interactions in Aqueous Solutions and Crystals, *Can. J. Chem.*, 1975, **53**, DOI:10.1139/v75-196.

7 M. U. Belyi, G. I. Gaididei, V. P. Sakun and M. G. Skryshevskaya, Concentration effects in the vibrational spectra of aqueous solutions of nitrites, *J. Appl. Spectrosc.*, 1995, **62**, 76–82.

8 M. H. Brooker and B. S. DeYoung, Measurement of the stability constants for aqueous calcium and magnesium nitrite by Raman spectroscopic methods, *J. Solution Chem.*, 1980, **9**, DOI:10.1007/BF00644553.

9 S. A. Al-Baldawi, M. H. Brooker, T. E. Gough and D. E. Irish, Raman, infrared, and proton magnetic resonance investigation of solutions of zinc nitrate in anhydrous methanol, *Can. J. Chem.*, 1970, **48**, DOI:10.1139/v70-198.

10 J. D. Riddell, D. J. Lockwood and D. E. Irish, Ion Pair Formation in $NaNO_3/D_2O$ Solutions: Raman and Infrared Spectra, Partial Molal Volumes, Conductance, and Viscosity, *Can. J. Chem.*, 1972, **50**, 2951–2962, DOI:10.1139/v72-474

11 J. Y. Yu, Y. Zhang, S. H. Tan, Y. Liu and Y. H. Zhang, Observation on the ion association equilibria in $NaNO_3$ droplets using micro-Raman spectroscopy, *J. Phys. Chem. B*, 2012, **41**, DOI:10.1021/jp306367v.

12 J. B. Gill, Solute-Solute Interactions in Liquid Ammonia Solutions: A Vibrational Spectroscopic View, *Pure Appl. Chem.*, 1981, **53**, DOI:10.1351/pac198153071365.

13 D. E. Irish and M. H. Brooker, Interactions and residence times in aqueous alkali metal nitrite solutions from Raman spectral measurements, Trans. *Faraday Soc.*, 1971, **67**, DOI:10.1039/TF9716701916.

14 A. G. Miller and J. A. Macklin, Matrix Effects on the Raman Analytical Lines of Oxyanions, *Anal. Chem.*, 1980, **52**, DOI:10.1021/ac50056a009.

15 E. O. Stejskal and J. E. Tanner, Spin diffusion measurements: Spin echoes in the presence of a time-dependent field gradient, *J. Chem. Phys.*, 1965, **42**, DOI:10.1063/1.1695690.

16 J. E. Tanner, Pulsed field gradients for NMR spin-echo diffusion measurements, *Rev. Sci. Instrum.*, 1965, **36**, DOI:10.1063/1.1719808.

17 H. Jacobs and U. Metzner, Ungewöhnliche H-Brückenbindungen in Natriumhydroxidmonohydrat: Röntgen- und Neutronenbeugung an $NaOH{\cdot}H_2O$ bzw. $NaOD{\cdot}D_2O$, *Zeitschrift für Anorg. und Allg. Chemie*, 1991, **597**, 97–106, DOI: 10.1002/ZAAC.19915970113.

18 H. -J Bleif and H. Dachs, Crystalline modifications and structural phase transitions of NaOH and NaOD, *Acta Crystallogr. Sect. A*, 1982, **38**, 470–476, DOI:10.1107/S0567739482001028.

19 T. Proffen and R. B. Neder, DISCUS: A program for diffuse scattering and defect-structure simulation, *J. Appl. Crystallogr.*, 1997, **30**, 171–175, DOI:10.1107/S002188989600934X.

20 C. L. Farrow, P. Juhas, J. W. Liu, D. Bryndin, E. S. Boin, J. Bloch, T. Proffen and S. J. L. Billinge, PDFfit2 and PDFgui: Computer programs for studying nanostructure in crystals, *J. Phys. Condens. Matter*, 2007, **19**, 335219(7pp), DOI:10.1088/0953-8984/19/33/335219.